Journal of Power Sources 245 (2014) 998–1004

Contents lists available at SciVerse ScienceDirect

Journal of Power Sources

journal homepage: www.elsevier.com/locate/jpowsour

# Oxygen reduction reaction over silver particles with various morphologies and surface chemical states

Junya Ohyama [a,b,*], Yui Okata [a], Noriyuki Watabe [a], Makoto Katagiri [a], Ayaka Nakamura [c], Hidekazu Arikawa [c], Ken-ichi Shimizu [b,c], Tatsuya Takeguchi [c], Wataru Ueda [c], Atsushi Satsuma [a,b,*]

[a] Graduate School of Engineering, Nagoya University, Nagoya 464-8603, Japan
[b] Elements Strategy Initiative for Catalysts and Batteries (ESICB), Kyoto University, Katsura, Kyoto 615-8520, Japan
[c] Catalysis Research Center, Hokkaido University, Sapporo 001-0021, Japan

## HIGHLIGHTS

- Morphology and surface chemical state of Ag powders affected the ORR activity.
- Defective and oxidized surface enhanced Ag active surface area during the ORR.
- Ag particles with defective and angular surfaces exhibited higher specific activity.

## GRAPHICAL ABSTRACT

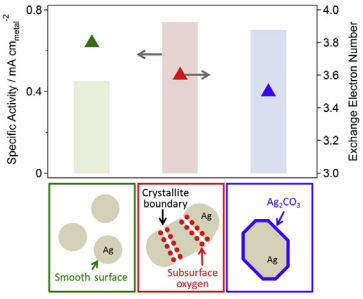


## ARTICLE INFO

*Article history:*
Received 11 April 2013
Received in revised form
4 July 2013
Accepted 6 July 2013
Available online 13 July 2013

*Keywords:*
Silver
Oxygen reduction reaction
Morphology
Surface chemical state
Raman spectroscopy

## ABSTRACT

The oxygen reduction reaction (ORR) in an alkaline solution was carried out using Ag powders having various particle morphologies and surface chemical states (Size: ca. 40–110 nm in crystalline size. Shape: spherical, worm like, and angular. Surface: smooth with easily reduced $AgO_x$, defective with $AgO_x$, and $Ag_2CO_3$ surface layer). The various Ag powders were well characterized by X-ray diffraction, X-ray photoelectron spectroscopy, $N_2$ adsorption, scanning electron microscopy, Raman spectroscopy, cyclic voltammetry, and stripping voltammetry of underpotential-deposited lead. Defective and oxidized surfaces enhanced the Ag active surface area during the ORR. The ORR activity was affected by the morphology and surface chemical state: Ag particles with defective and angular surfaces showed smaller electron exchange number between three and four but showed higher specific activity compared to Ag particles with smooth surfaces.



## 1. Introduction

Alkaline anion exchange membrane fuel cells (AAEMFCs) have attracted considerable attention owing to their potential for the application of non-Pt metals as electrode catalysts due to the less corrosive environment for the catalysts than proton exchange membrane fuel cells (PEMFCs) [1–7]. To achieve high oxygen reduction reaction (ORR) activity, comparable to Pt catalysts, various metals such as Ag [8–16], Au [3,13,17], Pd [12,18,19], Ni [20], and manganese oxides

* Corresponding authors. Graduate School of Engineering, Nagoya University, Nagoya 464-8603, Japan. Tel.: +81 52 789 3191; fax: +81 52 789 3193.
*E-mail addresses:* ohyama@apchem.nagoya-u.ac.jp (J. Ohyama), satsuma@apchem.nagoya-u.ac.jp (A. Satsuma).

0378-7753/$ – see front matter © 2013 Elsevier B.V. All rights reserved.
http://dx.doi.org/10.1016/j.jpowsour.2013.07.034

[16,21–24] have been studied. One effective strategy to enhance catalytic activity for the ORR is controlling the size of metal particles. For example, Chen et al. clearly presented the size-dependent ORR activity of Pd supported on carbon (Pd/C) by evaluation of the ORR activity normalized to the Pd active surface area and mass [12]. In their study, the highest ORR activity was observed on Pd particles (ca. 5 nm in diameter) supported on carbon when the size of Pd nanoparticles decreased from 16.7 to 3 nm. For Au catalysts, it has been reported that Au nanoclusters with a diameter less than 2 nm represented high ORR activity deviating from bulk Au behavior [17]. Li et al. represented that large Ag particles (174 nm in diameter) showed a four-electron reduction of oxygen, and fine Ag nanoparticles (4.1 nm in diameter) showed a large two-electron pathway contribution, which indicates that larger Ag particles reduce oxygen more efficiently [11]. On the other hand, a 2.3 electron ORR pathway on 20 wt% Ag/C with 47.7 nm of Ag particles and a 3.6 electron ORR pathway on 20 wt% Ag/C with 15 nm of Ag particles have been also reported [9,25]. Thus, it is evident that the effect of size on the ORR activity is still not well understood. This would be due to other factors related to the ORR, such as loading amount, morphology, and surface chemical state [8,10,16,21,26,27].

Among the non-Pt metals described above, Ag is regarded as the most promising metal to replace Pt owing to its abundance, relatively low cost, and high activity [3,6,8,10,28]. Interestingly, considering Ag catalysts for the ORR in a previous study, it was proposed that the redox property of the Ag catalyst is a controlling factor of the ORR catalytic activity [10,29]. It is assumed that the structure and surface chemical state of Ag affect the redox property and the ORR activity [29,30]. For other metal catalysts, the surface chemical state as well as the structure has an effect on the ORR activity [16,19,21,31–34]. However, few studies have investigated the effect of the surface chemical state of Ag on the ORR activity [30,35,36].

We investigated the effect of Ag morphology and surface chemical state on the ORR activity in alkaline solutions using various Ag particles well characterized by X-ray diffraction (XRD), $N_2$ adsorption, scanning electron microscopy (SEM), X-ray photoelectron spectroscopy (XPS), Raman spectroscopy, cyclic voltammetry (CV), and stripping voltammetry of underpotential-deposited lead ($Pb_{upd}$).

## 2. Experimental

### 2.1. Catalysts

Ag metal powders used in this study were purchased from Aldrich (Ag-A), Kojundo Chemical Lab. Co., Ltd. (Ag-K), and Kishida Chemical Co., Ltd. (Ag-KC). As a reference, a Ag/C catalyst with 60 wt% loading on a carbon black (CB) was purchased from E-Tek Co. (Ag/C-E). For electrochemical measurements, the Ag powders were physically mixed with Vulcan XC-72R CB (Cabot Corp.) to prepare Ag catalysts (Ag loadings: 60 wt% for Ag-A and Ag-K, 90 wt % for Ag-KC).

### 2.2. Characterization

XRD patterns of samples were recorded on a Rigaku MiniFlex II/AP diffractometer with Cu $K\alpha$ radiation. The crystallite size of the Ag powder was evaluated from the half-width of the Ag(111) line using the Scherrer equation after correcting for instrumental peak broadening using the half-width of Si(111) of silicon powder purchased from Kishida Chemical Co., Ltd. The Scherrer constant was assumed to be 0.9. The morphology of Ag particles was observed using a JEOL JSM-7500FA scanning electron microscope. XPS were acquired on a JPS-9000MC system (JEOL Ltd.) using Al $K\alpha$ radiation. Brunauer–Emmett–Teller (BET) specific surface area of Ag powders was measured by $N_2$ adsorption at 77 K on a BELSORP 28SA (Bel Japan, Inc.) instrument. Prior to measurements, each sample was outgassed at room temperature for 2 h.

Raman spectra were measured on a JASCO RMP-330 spectrophotometer equipped with a 532 nm green semiconductor laser as an excitation source. The samples were filled in an in situ diffuse reflectance cell having a quartz window (15 mm) and an internal heating system connected to a gas flow system [37]. A 20× objective optical lens was used to focus the depolarized laser beam on the sample surface and to collect the backscattered light. The backscattered light was dispersed by a single-stage spectrometer with 1800-groove $mm^{-1}$ grating and acquired by an air-cooled 1024 × 256 pixel charge-coupled device. The Raman scattering was collected in the spectral region of 89.28–1324.29 $cm^{-1}$ with a resolution of 1 $cm^{-1}$. The exposure time was 120 s for Ag-A, 5 s for Ag-K, and 60 s for Ag-KC, and five scans were accumulated for each spectrum. As references, the spectra of $Ag_2O$ and $Ag_2CO_3$ were purchased from Kishida Chemical Co., Ltd. and Mitsuwa Chemical Co., Ltd., respectively. The sample was filled in the cell and measured at room temperature. The in situ Raman spectra were collected under 20 mL $min^{-1}$ $H_2$ flow at a given temperature.

### 2.3. Cyclic voltammetry, $Pb_{upd}$ stripping voltammetry, and the ORR measurement

Cyclic voltammograms (CVs), $Pb_{upd}$ stripping voltammograms, and linear sweep voltammograms for the ORR were obtained using the rotating disk electrode (RDE) setup with a potentiostat (HZ-5000 (HAG-3001), Hokuto Denko Corp.).

Catalyst ink was prepared by ultrasonic mixing of a suspension of 10–20 mg of catalysts in a mixed solution of 1 mL of 1-hexanol and 21.7 μL of an ionomer solution (AS-4 solution (5 wt% in 1-propanol, Tokuyama Corp.)). The catalyst ink was dropped on the glassy carbon substrate of the RDE (HR2-D1-GC-5, 5 mm in diameter, 0.196 $cm^2$, Hokuto Denko Corp.) in 2.5–5 μL. After the ink was dried on the substrate, 7 μL of a diluted ionomer solution (0.05 wt% in 1-propanol) was dropped on the disk.

The ORR was carried out in an $O_2$-purged 0.1 M NaOH aqueous solution using a three-electrode cell with a Pt wire counter electrode and a Hg/HgO/0.1 M NaOH ($Hg/HgO/OH^-$) reference electrode. After the NaOH solution was saturated with $O_2$ gas by purging for at least 0.5 h, the ORR was recorded by sweeping the potential from 0.2 to −0.8 V vs $Hg/HgO/OH^-$ at 20 mV $s^{-1}$ at 293 K. CV and $Pb_{upd}$ stripping voltammetry were performed in a $N_2$-purged 0.1 M NaOH solution and the solution containing 125 μM $Pb(NO_3)_2$, respectively, (10 mV $s^{-1}$, 293 K). The $Pb_{upd}$ strip voltammogram was obtained after Pb deposition at −0.7 V vs $Hg/HgO/OH^-$ for 300 s.

## 3. Results and discussion

### 3.1. Physical characterization

Table 1 lists the crystallite size evaluated by XRD (Fig. S1) and the BET surface area ($SA_{BET}$) of Ag-A, Ag-K, and Ag-KC. The order of crystallite size was Ag-A (38 nm) < Ag-K (62 nm) < Ag-KC (113 nm). Ag powders with smaller crystallite size exhibited larger BET surface area values. Fig. 1 shows typical SEM images of Ag powders used in this study. Ag-A exhibited spherical and relatively monodispersed particles ca. 50 nm in diameter (Fig. 1(a)). Ag-K was composed of variously sized (ca. 10 nm–1 μm) particles having a worm-like shape (Fig. 1(b)). Ag-KC particles had angular shape and various sizes (ca. 50 nm to 2 μm) (Fig. 1(c)). The particle size of Ag-A observed by SEM (ca. 50 nm) was comparable to the crystallite size evaluated by XRD (38 nm); however, those of Ag-K and Ag-KC were different from the corresponding crystallite sizes. It is likely that the

**Table 1**
Results of physical and electrochemical characterization of Ag powders used in this study.

| Ag powder | Crystallite size (nm)[a] | $SA_{BET}$ ($m^2\ g^{-1}$)[b] | Particle morphology and surface chemical state[c] | ESA ($m^2\ g^{-1}$)[d] | $ESA/SA_{BET}$ (%)[e] |
|---|---|---|---|---|---|
| Ag-A | 38 | 4.7 | Spherical particle with easily reduced $AgO_x$ species on smooth surface | 4.2 | 90 |
| Ag-K | 62 | 2.5 | Worm-like particle with subsurface oxygen at surface defect | 3.5 | 142 |
| Ag-KC | 113 | 0.5 | Angular particle with surface $Ag_2CO_3$ layer and defect | 0.6 | 122 |

[a] Evaluated from XRD line width of Ag(111) using Scherrer equation.
[b] BET surface area.
[c] Analyzed by CV, SEM observation, and Raman spectroscopy.
[d] Electrochemically active surface area determined by $Pb_{upd}$ stripping voltammetry.
[e] The ratio of ESA to $SA_{BET}$.

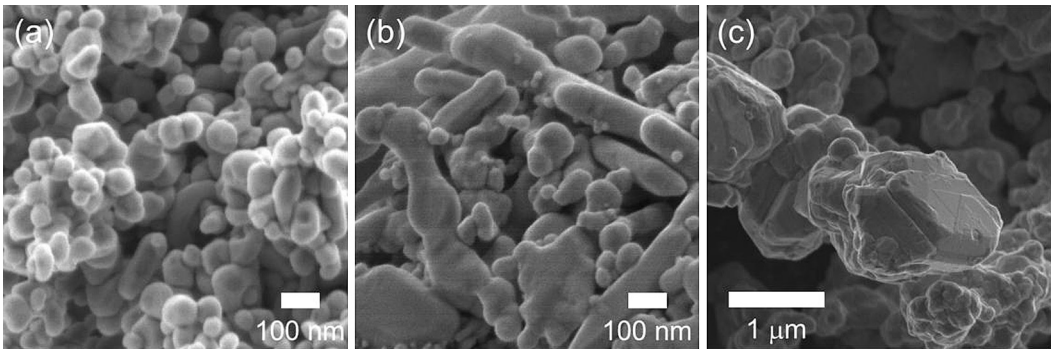


**Fig. 1.** Typical SEM images of (a) Ag-A, (b) Ag-K, and (c) Ag-KC.

Ag-K and Ag-KC particles were composed of 62 and 113 nm Ag crystallites, respectively, as evaluated by XRD.

Fig. 2 shows Ag 3d XPS of the Ag powders. The Ag $3d_{5/2}$ XPS peak binding energy of Ag-A was 368.2 eV, which is consistent with the previously reported peak energy of Ag metal [38,39]. On the other hand, the Ag $3d_{5/2}$ peak energies of Ag-K and Ag-KC were lower than Ag-A (367.6 and 368.0 eV, respectively). It has been reported that Ag oxides (and $Ag_2CO_3$) present peaks at lower binding energy [38,39]. Thus, the XPS analysis indicated that Ag-K and Ag-KC were in a more oxidized state than Ag-A.

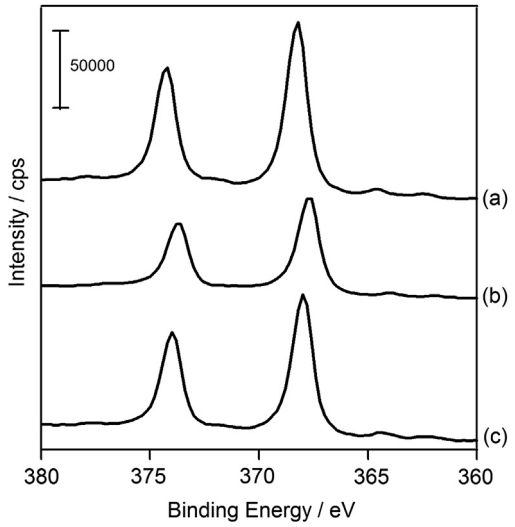


**Fig. 2.** Ag 3d XPS of (a) Ag-A, (b) Ag-K, and (c) Ag-KC.

Fig. 3 shows the Raman spectra of Ag powders used in this study. $Ag_2O$ and $Ag_2CO_3$ are used as references. The Raman spectrum of Ag-K exhibited an intense band around 661 $cm^{-1}$ and small bands around 485, 758, and 960 $cm^{-1}$ (Fig. 3(b)). We assigned the band at 661 $cm^{-1}$ to subsurface oxygen species in the vicinity of defects and the other small bands around 485, 758, and 960 $cm^{-1}$ to dissolved atomic oxygen in the silver lattice, $Ag^{III}$=O species, and adsorbed

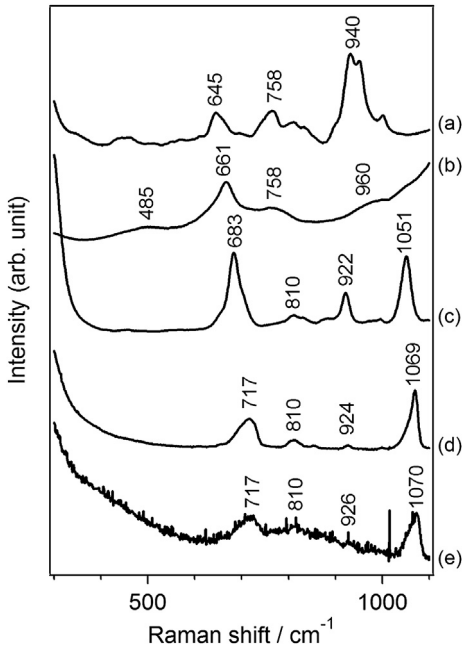


**Fig. 3.** Raman spectra of (a) Ag-A, (b) Ag–K, and (c) Ag-KC, together with (d) $Ag_2CO_3$ and (e) $Ag_2O$ as references.

$O_2^-$ species, respectively, although the bands appeared at a different Raman shift from those of previous reports [40–44]. This difference is possibly due to the difference in morphology (size and shape) between Ag-K and previously reported Ag metal. The Raman spectrum of Ag-A powder exhibited a relatively intense band around 940 $cm^{-1}$, which is attributable to adsorbed $O_2^-$ and small bands around 645 and 758 $cm^{-1}$, which are attributable to subsurface oxygen species and $Ag^{III}$=O species, respectively (Fig. 3(a)). The Raman bands of Ag-A were much weaker than those of Ag-K (Fig. S2). In particular, the band around 661 $cm^{-1}$ of Ag-K was (ca. 25 times larger than that around 645 $cm^{-1}$ of Ag-A). It has been reported that an intense band derived from subsurface oxygen species in the vicinity of defects was observed on a Ag catalyst having a highly defected structure and not on that with smooth structures. Thus, the much higher intensity of the band around 661 $cm^{-1}$ of Ag-K than that of Ag-A indicates a highly defected structure and a large amount of subsurface oxygen species for Ag-K compared to Ag-A, although accurate results are not possible owing to the limitations of surface-enhanced Raman spectroscopy [40]. Transmission electron microscopy analysis also showed the defective worm-like structure of Ag-K and the spherical smooth surface of Ag-A (Fig. S3). Compared to Ag-A, the $AgO_x$ species on Ag-K were stable to heat under $H_2$ flow (Fig. 4). In other words, oxygen species in the boundary of the Ag particle or a defected structure are more stable than those in a Ag particle with a smooth surface [40]. For Ag-KC, the Raman spectrum contained bands at approximately the same Raman shifts as those of $Ag_2CO_3$ (Fig. 3(c) and (d)); comparable bands were also observed on the spectrum of as purchased $Ag_2O$ (Fig. 3(e)). The Raman spectrum of treated $Ag_2O$ is shown in Fig. S4. Ag-KC might have a $Ag_2O$ layer adsorbing $CO_2$, although the resulting $Ag_2CO_3$ layer was not detected by XRD (Fig. S1). Table 1 summarizes the results of physical characterization of the Ag powders.

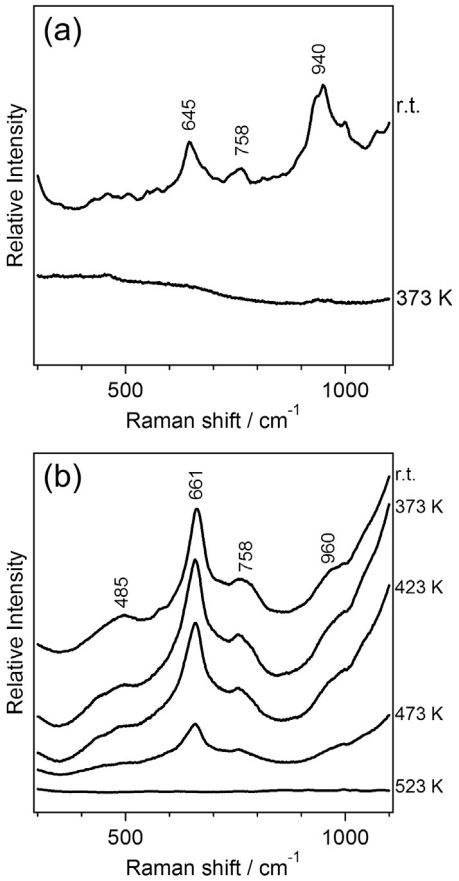


**Fig. 4.** In situ Raman spectra obtained on (a) Ag-A and (b) Ag-K under $H_2$ flow at various temperatures.

### 3.2. Electrochemical characterization

Fig. 5 shows the CVs of Ag catalysts in a $N_2$ saturated 0.1 M NaOH aqueous solution. All Ag catalysts exhibited three anodic peaks and a cathodic peak. The feature of CVs, particularly of the anodic curve, was different from each other. The anodic curve had three peaks derived from silver dissolution and the formation of a surface monolayer of $Ag_2O$ films at ca. 0.23 V (denoted as $A_1$), the formation of AgOH at ca. 0.30 V ($A_2$), and the formation of $Ag_2O$ at ca. 0.38 V ($A_3$) (Table S1). The Ag-A anodic curve was well consistent with that of previously reported Ag spherical nanoparticles [10,30] which agree with the result of physical characterization by SEM and Raman spectroscopy. Ag-K presented smaller peak current ratios of $A_1/A_3$ and $A_2/A_3$ than Ag-A (Table S1), and the anodic curve was similar to that of polycrystalline Ag reported elsewhere. Thus, in the case of Ag-K, the CV analysis results supported the physical characterization that Ag-K had defected structures and angular shapes. The CV of Ag-KC was similar to that of Ag-K. It is suggested that Ag-KC with angular shapes and $Ag_2CO_3$ on the surface has defective structures. On the basis of these results, it is reasonable to conclude that the surfaces of Ag-K and Ag-KC are more defective than Ag-A.

Fig. 6 shows $Pb_{upd}$ stripping voltammograms for the series of Ag catalysts [45]. The $Pb_{upd}$ stripping and deposition reaction on Ag in alkaline solutions can be represented as follows.

$$Pb_{upd} + 3OH^- \rightleftarrows HPbO_2^- + H_2O + 2e^-$$

It should be noted that the CVs of Ag catalysts (Fig. 5) do not exhibit redox peaks in the potential range of $Pb_{upd}$ stripping voltammograms (Fig. 6). Thus, the anodic and cathodic peaks shown in Fig. 6 are derived from the stripping and deposition of Pb, respectively. The $Pb_{upd}$ stripping curves (anodic curves) of the Ag catalysts show two representative peaks at ca. −0.50 (denoted as $S_1$) and −0.55 V ($S_2$) vs Hg/HgO/$OH^-$. The feature of the voltammogram was similar to that of Ag nanoparticles in 0.1 M KOH aqueous solutions, as reported previously [35]. The three catalysts exhibited different ratios of $S_1$ to $S_2$ peak current of the anodic curves. More specifically, Ag-A exhibited the highest peak current ratio, and Ag-K showed the lowest. It is possible that $S_1$ and $S_2$ are derived from smooth and defective surfaces, respectively.

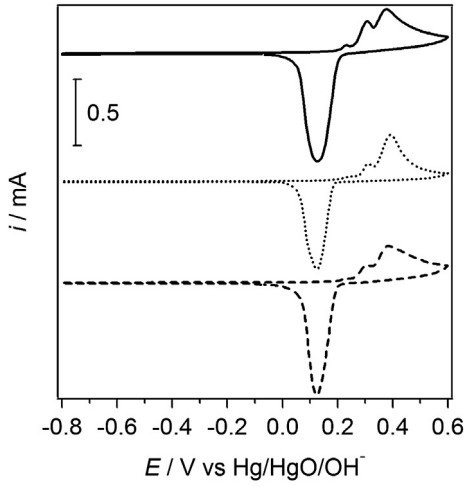


**Fig. 5.** Cyclic voltammograms of Ag-A (solid), Ag-K (dotted), and Ag-KC (dashed) in $N_2$ saturated 0.1 M NaOH aqueous solution. Scan rate: 10 mV $s^{-1}$. The amount of Ag metal on a disk electrode of Ag-A: 30 μg; Ag-K: 15 μg; Ag-KC: 90 μg.

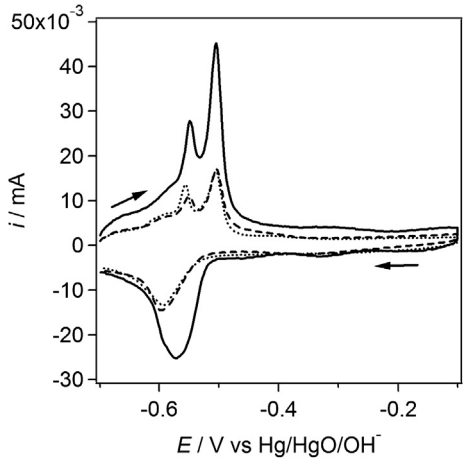


**Fig. 6.** Strip voltammograms of $Pb_{upd}$ on Ag-A (solid), Ag-K (dotted), and Ag-KC (dashed) in $N_2$ saturated 0.1 M NaOH + 125 μM $Pb(NO_3)_2$ solution. Scan rate: 10 mV $s^{-1}$. The amount of Ag metal on a disk electrode of Ag-A: 30 μg; Ag-K: 15 μg; Ag-KC: 90 μg.

The electrochemically accessible surface area (ESA) of Ag catalysts was determined from underpotential-deposited lead ($Pb_{upd}$) because Ag is inactive for the deposition and stripping of CO and $H_{upd}$ which is a standard technique for surface area determination of a Pt catalyst. The ESAs of the Ag catalysts were evaluated from the anodic peak area, i.e., the stripping charge of $Pb_{upd}$ using 260 μC $cm^{-2}$ of charge density (Fig. S5) [8,35,46,47]. The calculated ESAs are listed in Table 1. The ESA of Ag-A was slightly smaller than the corresponding $SA_{BET}$. However, it is interesting to note that for Ag-K and Ag-KC, the ESAs were larger than the $SA_{BET}$. In fact, the ratio of ESA to $SA_{BET}$ ($ESA/SA_{BET}$) decreased in the order of Ag-K > Ag-KC > Ag-A, and $ESA/SA_{BET}$ of Ag-K and Ag-KC was more than 100%. The physical characterization described above indicates that Ag-K and Ag-KC have surface oxygen species in the defected structure and the $Ag_2CO_3$ surface layer, respectively. However, Ag-A has a smooth surface and easily reduced $AgO_x$ species (Table 1). These oxidized Ag species would be reduced in the ORR measurement according to the Pourbaix diagrams [48]. Thus, Ag species with an oxidized surface and/or defect increases the ESA during the electrochemical measurement. It is suggested that such Ag surfaces induce a roughened surface and/or decomposition into small Ag particles. These results indicate that the ESA is accurate for the Ag surface area during the ORR; however, BET is not. Therefore, we used the ESA in the following evaluation of the ORR activity.

### 3.3. ORR measurement

The ORR measurements were performed using the Ag powders in an oxygen saturated 0.1 M NaOH aqueous solution. Fig. 7(a) shows the oxygen reduction polarization curves obtained on Ag-A, Ag-K, and Ag-KC physically mixed with CB. The Ag loading of Ag-A and Ag-K was 60 wt%. However, the Ag loading of Ag-KC was 90 wt% because its low Ag surface area increases catalyst thickness on a disk electrode, which prevents proper evaluation of catalytic activity for the ORR [46]. The amounts of Ag catalysts on a RDE were optimized according to a recent report by Markovic et al. (Fig. S6) [46].

We calculated the mass activity ($j_M$) of the Ag catalysts by normalization of the current at −0.2 V vs $Hg/HgO/OH^-$ ($i_{-0.2\,V}$) with Ag weight on a disk electrode. As a reference, the ORR was also conducted using commercial Ag/C with 60 wt% Ag loading (E-Tek), which is denoted as Ag/C-E (Fig. S7: the ORR curve. Fig. S8: $Pb_{upd}$ strip voltammogram; 1.5 $m^2\,g^{-1}$ of ESA. Fig. S1: XRD; 79 nm of crystallite size. Fig. S9: SEM image.), and $j_M$ was calculated [3]. The $j_M$ value decreased in the order of Ag-K (19.7 mA $mg_{Ag}^{-1}$) ≥ Ag-A (12.3 mA $mg_{Ag}^{-1}$) > Ag/C-E (7.7 mA $mg_{Ag}^{-1}$) > Ag-KC (3.3 mA $mg_{Ag}^{-1}$), which was consistent with crystallite size. It is noteworthy that Ag-A and Ag-K physically mixed with CB showed higher $j_M$ than commercially available Ag/C-E catalysts (1.6 and 2.6 times, respectively).

The catalytic activity per Ag surface area was evaluated from the potential at −25 μA $cm_{Ag}^{-2}$ of ESA-normalized current density, as shown in Fig. 7(b) [7]. Here we did not use $SA_{BET}$ to calculate the specific activity because, as described above, the metal surface area would change under the ORR measurement. As a result, the potential decreased in the order of Ag-K ≈ Ag-KC > Ag-A. The result indicates that the catalytic activity per Ag surface area decreased in the order of Ag-K ≈ Ag-KC > Ag-A. For further inspection of the catalytic activity, mass-transfer independent kinetics for the ORR on the three well-characterized Ag catalysts were calculated using the Koutecky–Levich (K–L) equation:

$$\frac{1}{j} = \frac{1}{j_k} + \frac{1}{j_d} = \frac{1}{nFkc_0} + \frac{1}{0.62nFD^{2/3}\nu^{-1/6}c_0\omega^{1/2}}$$

where $j_k$ and $j_d$ are the kinetic and diffusion limited current densities, $n$ is the exchange electron number, $k$ is the kinetic constant, $F$ is the Faraday constant, $D$ is the $O_2$ diffusion coefficient in 0.1 M

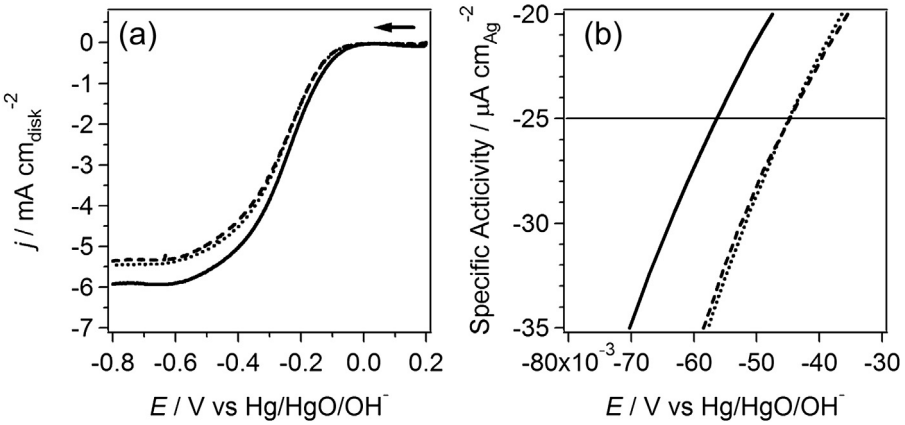


**Fig. 7.** (a) Oxygen reduction polarization curves obtained on Ag-A (solid), Ag-K (dotted), and Ag-KC (dashed) in $O_2$ saturated 0.1 M NaOH aqueous solution. Rotation rate: 2500 rpm. Scan rate: 20 mV $s^{-1}$. The amount of Ag metal on a disk electrode of Ag-A: 30 μg; Ag-K: 15 μg; Ag-KC: 90 μg. The current density ($j$) was calculated using the geometric surface area of a rotating disk electrode. (b) ESA-normalized current density ($j_s$) of Ag-A (solid), Ag-K (dotted), and Ag-KC (dashed). The potentials at −25 μA $cm_{Ag}^{-2}$ is a benchmark for comparison [7].

**Table 2**
Specific activity ($j_{k:ESA}$) and exchange electron number ($n$) for the ORR.

| Catalyst | $j_{k:ESA}$ (mA $cm_{Ag}^{-2}$)[a] | $n$[b] |
|---|---|---|
| Ag-A | 0.45 | 3.8 |
| Ag-K | 0.74 | 3.6 |
| Ag-KC | 0.70 | 3.5 |

[a] Calculated from the intercept of the line fitted to the Koutecky–Levich (K–L) plot for $j_{-0.2\ V}$ (Fig. S10). $j_{k:ESA} = j_k \times A/(ESA \times wt_{Ag})$, where $wt_{Ag}$ is the Ag weight on a disk electrode, and $A$ is the area of disk electrode (0.196 $cm^2$).
[b] Calculated from the slope of the K–L plot for $j_{-0.5\ V}$ (Fig. S10).

NaOH ($1.93 \times 10^{-5}$ $cm^2$ $s^{-1}$), $\nu$ is the kinematic viscosity ($1.09 \times 10^{-2}$ $cm^2$ $s^{-1}$), $c_0$ is the $O_2$ concentration in electrolyte ($1.26 \times 10^{-6}$ mol $cm^{-3}$), and $\omega$ is the rotation rate in the radian [49]. The $j_k$ value was calculated from the intercept of the line fitted to the K–L plot for $j$ at −0.2 V vs Hg/HgO/$OH^-$ (Fig. S10). The specific activity ($j_{k:ESA}$) was obtained using the ESA ($j_{k:ESA} = i_k/ESA = j_k A/ESA$, where $A$ is the area of the disk electrode), as shown in Table 2. The $j_{k:ESA}$ value decreased in the order of Ag-K ≥ Ag-KC > Ag-A, which is consistent with the order of the potential at −25 μV $cm_{Ag}^{-2}$ (Fig. 7(b)). It should be noted that the $j_{k:ESA}$ value does not depend on Ag particle size. The Ag size investigated in this study (>10 nm) has an insignificant effect on the specific activity, although much smaller Ag particles (<3 nm) might show unique size-dependent activity due to the large fraction of coordinatively unsaturated Ag atoms and quantum size effect. From the K–L plot for $j$ at −0.5 V vs Hg/HgO/$OH^-$ ($j_{-0.5\ V}$), the electron exchange numbers ($n$) for Ag-A, Ag-K, and Ag-KC were determined to be 3.8, 3.6, and 3.5, respectively (Table 2). The reason for the difference in the $j_{k:ESA}$ and $n$ values between the Ag catalysts is discussed below.

The exchange electron numbers for all Ag catalysts were close to but slightly less than four. The $n$ values were comparable to those previously reported by Buttry et al., who showed slightly less than a four-electron pathway using Ag nanoparticles and polycrystalline Ag [8]. In the present study, the $n$ value decreased in the order of Ag-A > Ag-K ≥ Ag-KC. In other words, the fraction of the two-electron pathway on Ag-K and Ag-KC is larger compared to that on Ag-A. The physical and electrochemical characterization indicates that Ag-K with subsurface oxygen species and Ag-KC with $Ag_2CO_3$ have defective surfaces. Therefore, the defective and oxidized surfaces of Ag-A and Ag-KC cause the two-electron pathway. It has been reported that strongly adsorbed $OH_{ad}$ on a defective surface decreases the neighboring Ag sites to adsorb $O_2$ with both O, which results in an increase in the fraction of the two-electron pathway [8].

As described above, the $j_{k:ESA}$ value decreased in the order of Ag-K ≥ Ag-KC > Ag-A (Table 2). This was due to higher affinity with $O_2$ for Ag-K and Ag-KC than for Ag-A. Previously, Blizanac et al. showed that the activation energy for the ORR is surface structure sensitive [36]. Buttry et al. showed a higher rate constant on polycrystalline Ag with a defective surface than Ag nanoparticles with a smooth surface [8]. On the basis of these results, we propose that the defective and oxidized surface of Ag-K and Ag-KC can more strongly adsorb $O_2$ and can conduct the first charge-transfer with lower activation energy than Ag-A with a smooth surface.

## 4. Conclusions

The effect of the Ag particle morphology and surface chemical state on the ORR was investigated using various well-characterized Ag powders.

Ag catalysts having $AgO_x$ on a defective surface and $Ag_2CO_3$ surface layer demonstrated more than 100% of $ESA/SA_{BET}$, which was higher than that having easily reduced $AgO_x$ on a smooth surface. It is assumed that the defective surface and the oxidized species induce a roughened surface and/or decompose into small Ag particles during the ORR, thereby causing an increase of ESA.

All Ag powders physically mixed with CB exhibited close to a four-electron pathway for the ORR. However, the Ag particles with defective and angular surfaces showed smaller $n$ values than those with smooth surfaces. It is strongly suggested that the defective and oxidized ($AgO_x$ or $Ag_2CO_3$) surface decreases the number of Ag neighboring sites required for a four-electron pathway. On the other hand, due to high affinity for $O_2$, Ag particles with defective and oxidized surfaces represented higher specific activity than those with smooth surfaces.

## Acknowledgment

This study was supported by Grant-in-Aid from the Ministry of Education, Culture, Sports, Science and Technology, Japan (MEXT) program “Elements Strategy Initiative to Form Core Research Center” (since 2012) and by a project of the New Energy and Industrial Technology Development Organization (NEDO) Japan, “Rare Metal Substitute Materials Development”. The authors thank Tokuyama Corp. for supplying ionomer solution (AS-4 solution).

## Appendix A. Supplementary data

Supplementary data related to this article can be found at http://dx.doi.org/10.1016/j.jpowsour.2013.07.034.

## References

[1] S.F. Lu, J. Pan, A.B. Huang, L. Zhuang, J.T. Lu, Proc. Natl. Acad. Sci. U. S. A. 105 (2008) 20611.
[2] J.R. Varcoe, R.C.T. Slade, Fuel Cells 5 (2005) 187.
[3] J.R. Varcoe, R.C.T. Slade, G.L. Wright, Y.L. Chen, J. Phys. Chem. B 110 (2006) 21041.
[4] H. Bunazawa, Y. Yamazaki, J. Power Sources 182 (2008) 48.
[5] J.S. Spendelow, A. Wieckowski, Phys. Chem. Chem. Phys. 9 (2007) 2654.
[6] J.-S. Park, S.-H. Park, S.-D. Yim, Y.-G. Yoon, W.-Y. Lee, C.-S. Kim, J. Power Sources 178 (2008) 620.
[7] J. Suntivich, H.A. Gasteiger, N. Yabuuchi, H. Nakanishi, J.B. Goodenough, Y. Shao-Horn, Nat. Chem. 3 (2011) 546.
[8] P. Singh, D.A. Buttry, J. Phys. Chem. C 116 (2012) 10656.
[9] L. Demarconnay, C. Coutanceau, J.M. Léger, Electrochim. Acta 49 (2004) 4513.
[10] J. Guo, A. Hsu, D. Chu, R. Chen, J. Phys. Chem. C 114 (2010) 4324.
[11] J.-J. Han, N. Li, T.-Y. Zhang, J. Power Sources 193 (2009) 885.
[12] L. Jiang, A. Hsu, D. Chu, R. Chen, J. Electrochem. Soc. 156 (2009) B643.
[13] L. Kuai, B.Y. Geng, S.Z. Wang, Y.Y. Zhao, Y.C. Luo, H. Jiang, Chem. Eur. J. 17 (2011) 3482.
[14] Y. Lu, W. Chen, J. Power Sources 197 (2012) 107.
[15] C. Tan, F. Wang, J. Liu, Y. Zhao, J. Wang, L. Zhang, K.C. Park, M. Endo, Mater. Lett. 63 (2009) 969.
[16] Q.E. Tang, L.H. Jiang, J. Qi, Q. Jiang, S.L. Wang, G.Q. Sun, Appl. Catal. B Environ. 104 (2011) 337.
[17] W. Chen, S.W. Chen, Angew. Chem. Int. Ed. 48 (2009) 4386.
[18] L. Jiang, A. Hsu, D. Chu, R. Chen, Electrochim. Acta 55 (2010) 4506.
[19] M. Shao, T. Yu, J.H. Odell, M. Jin, Y. Xia, Chem. Commun. 47 (2011) 6566.
[20] S.N.S. Goubert-Renaudin, A. Wieckowski, J. Electroanal. Chem. 652 (2011) 44.
[21] L. Mao, D. Zhang, T. Sotomura, K. Nakatsu, N. Koshiba, T. Ohsaka, Electrochim. Acta 48 (2003) 1015.
[22] W. Sun, A. Hsu, R.R. Chen, J. Power Sources 196 (2011) 627.
[23] T. Takakuwa, T. Kenko, M. Saito, H. Daimon, A. Tasaka, M. Inaba, H. Shiroishi, T. Hatai, J. Kuwano, ECS Trans. 41 (2011) 2185.
[24] N. Ohno, Y. Akeboshi, M. Saito, J. Kuwano, H. Shiroishi, T. Okumura, Y. Uchimoto, Top. Catal. 52 (2009) 903.
[25] F.H.B. Lima, C.D. Sanches, E.A. Ticianelli, J. Electrochem. Soc. 152 (2005) A1466.
[26] S. Guo, S. Zhang, L. Wu, S. Sun, Angew. Chem. Int. Ed. 51 (2012) 11770.
[27] H. Wu, W. Chen, J. Am. Chem. Soc. 133 (2011) 15236.
[28] P. Singh, K.L. Parent, D.A. Buttry, J. Am. Chem. Soc. 134 (2012) 5610.
[29] L. Nagle, A. Ahern, D. Burke, J. Solid State Electrochem. 6 (2002) 320.
[30] V. Bansal, V. Li, A.P. O'Mullane, S.K. Bhargava, CrystEngComm 12 (2010) 4280.
[31] J. Guo, H. Li, H. He, D. Chu, R. Chen, J. Phys. Chem. C 115 (2011) 8494.
[32] J. Kim, S.W. Lee, C. Carlton, Y. Shao-Horn, J. Phys. Chem. Lett. 2 (2011) 1332.
[33] K. Matsuzawa, T. Fukushima, M. Inaba, Electrocatalysis 1 (2010) 169.
[34] A. Toge, T. Yokono, M. Saito, H. Daimon, A. Tasaka, M. Inaba, ECS Trans. 41 (2011) 2283.

[35] G.K.H. Wiberg, K.J.J. Mayrhofer, M. Arenz, Fuel Cells 10 (2010) 575.
[36] B.B. Blizanac, P.N. Ross, N.M. Markovic, J. Phys. Chem. B 110 (2006) 4735.
[37] A. Satsuma, J. Shibata, A. Wada, Y. Shinozaki, T. Hattori, M.O. Masakazu Anpo, Y. Hiromi, Studies in Surface Science and Catalysis, vol. 145, Elsevier, 2003, p. 235.
[38] N. Ikeo, Y. Iijima, N. Nimura, M. Sigematsu, T. Tazawa, S. Matsumoto, K. Kojima, Y. Nagasawa, Handbook of X-ray Photoelectron Spectroscopy, JEOL, 1991.
[39] C.D. Wagner, W.M. Riggs, L.E. Davis, J.F. Moulder, Handbook of X-ray Photoelectron Spectroscopy, Perkin-Elmer Corp., 1979.
[40] G.J. Millar, J.B. Metson, G.A. Bowmaker, R.P. Cooney, J. Chem. Soc. Faraday Trans. 91 (1995).
[41] X. Bao, M. Muhler, B. Pettinger, R. Schlögl, G. Ertl, Catal. Lett. 22 (1993) 215.
[42] G.I.N. Waterhouse, G.A. Bowmaker, J.B. Metson, Appl. Surf. Sci. 214 (2003) 36.
[43] B. Pettinger, X. Bao, I.C. Wilcock, M. Muhler, G. Ertl, Phys. Rev. Lett. 72 (1994) 1561.
[44] G.I.N. Waterhouse, G.A. Bowmaker, J.B. Metson, Phys. Chem. Chem. Phys. 3 (2001) 3838.
[45] E. Herrero, L.J. Buller, H.D. Abruna, Chem. Rev. 101 (2001) 1897.
[46] K.J.J. Mayrhofer, D. Strmcnik, B.B. Blizanac, V. Stamenkovic, M. Arenz, N.M. Markovic, Electrochim. Acta 53 (2008) 3181.
[47] E. Kirowa-Eisner, Y. Bonfil, D. Tzur, E. Gileadi, J. Electroanal. Chem. 552 (2003) 171.
[48] M. Pourvaix, Atlas of Electrochemical Equilibria in Aqueous Solutions, Pergamon Press, Oxford, 1966.
[49] A.J. Bard, L.R. Faulkner, Electrochemical Methods: Fundamentals and Applications, Willey, New York, 2001.